Tampere University

Leonardo de Oliveira Negri

IMPACT OF AUTOMOBILE EXHAUST EMISSIONS ON AEROSOL AND GAS CONCENTRATIONS DURING THE SARS-COV-2 LOCKDOWN IN CENTRAL TAMPERE

An analysis of Black Carbon, LDSA and Air Quality

Bachelor's Thesis
Faculty of Engineering and Natural Sciences
Panu Karjalainen
Laeticia Petit
11/2020

ABSTRACT

Leonardo de Oliveira Negri: Research Assistant
Bachelor's Thesis
Tampere University
Bachelor's Degree in science and Engineering
November 2020

Traffic during the COVID-19 pandemic was affected by the lockdown measures taken to combat the spread of the disease. It was an opportunity to get unique measurements of particle formation by traffic and, in the future, compare the results with the normalized traffic.

For this purpose, the Aerosol Laboratory assembled instruments the Atmospheric and Trace gas Mobile Laboratory (ATMo-Lab) capable of analysing particle concentrations, particle distributions, and CO_2 and NO_x concentrations. Measurements were collected over the course of 24/04/2020 to 15/05/2020 during weekdays from approximately 8am to 5pm by driving in traffic and collecting particles through a front mounted inlet.

Results show high concentrations of Black Carbon and LDSA in the closed areas and numbers similar to the baseline urban background measurements. Considering the broad distribution of concentration, we cannot draw further conclusions about emission factors since the background measurements are well within uncertainty. North and South Tunnel, however, showed promise in estimating the value of the emissions on average by the fleet of cars with a total particle mass of 4.88µg/mg of CO2 and 4.25µg/mg of CO2 respectively at PM1.

The concentration of black carbon is also of note. The background value of 0.4864 $\mu g/m^3$ is well below large cities like New York and São Paulo, but the values on the North and South tunnel of 6.83 $\mu g/m^3$ and 4.35 $\mu g/m^3$ respectively are comparable to the BC levels in those cities, which might be a point of concern for public health.

PREFACE

I would like to thank everyone at the Aerosol Lab in Tampere University for warmly welcoming me in the team. Your help has been invaluable in my academic pursuits and had a very positive impact in my personal life as well.

I would also like to thank the support and funding provided by Business Finland with the Black Carbon Footprint project and by the Academy of Finland with the EFFi project.

Special thanks to Panu, Teemu, Sampsa and Laura for all their help analysing and processing the data during summer 2020 as well as giving me direction and feedback for the project.

Tampere, 22 Match 2021

Leonardo Negri

CONTENTS

LIST OF FIGURES

LIST OF SYMBOLS AND ABBREVIATIONS

ATMo-Lab	Atmospheric and Trace gas Mobile Laboratory
TUNI	Tampere University
CPC	Condensation Particle Counter
PSM	Particle Size Magnifier
ELPI+	Electrical Low Pressure Impactor
AE33	Magee Aethalometer© Model AE33
MA200	microAeth® Micro Aethalometer
AMS	Aerosol Mass Spectrometer
NOx	Nitrogen Oxides
UFP	Ultra-fine particles
HEPA Filter	High-Efficiency Particulate Air Filter
BC	Black Carbon
LDSA	Lung Deposition Surface Area

fA	femtoampere
$\mu m^2/cm^3$	micrometers per cubic centimeter
m	*mass*
PPB	Parts Per Billion
PPM	Parts Per Million

1. INTRODUCTION

Air quality is a topic of increasing interest for public health since it is linked with the increase of respiratory problems, infections, heart disease and others. [1] Anthropological air pollution is also well studied as the main contributor to Climate Change and, besides the known effects of CO_2 on the climate, aerosols also have a large impact on the climate and weather patterns. They influence scattering of light and the formation of clouds and, thus, influence weather patterns [2]. Our analysis has a specific focus on soot, also referred to as Black Carbon (BC), which has a secondary effect of lowering the albedo of ice, thus increasing the energy absorption of the planet [3] [4].

One of the main sources of air pollution in urban environments comes from automobile exhausts [5]. During the COVID-19 lockdowns, the traffic was greatly affected by the lockdown measures, seeing a monthly reduction of approximately 30% of traffic in the Tampere University Hospital Region in the height of the lockdowns in April 2020 [6]. These lockdowns had the intent of halting the spread of the disease. During this time, the Aerosol Physics Laboratory in Tampere University (TUNI) saw a unique opportunity to study exhaust particle and gas emissions.

For this purpose, the Atmospheric and Trace Gas Mobile Laboratory (AtMo-Lab) was outfitted with state-of-the-art equipment to measure aerosolized particles in central Tampere. The route planned included different urban environments so that we could have a broad range of measurements. We also outfitted the AtMo-Lab with instruments that could detect particles generated by the internal combustion of hydrocarbons in cars. These instruments measured Black Carbon (BC) or colloquially referred to as soot. We also measured Lung Deposition Surface Area (LDSA), CO_2 and Nitrous Oxides (NO_x) concentrations, particle number concentrations, particle size distributions, and calculated emission factors from the available data.

The instruments used for the experiment were the Condensation Particle Counter (CPC), for particle concentrations, the Dekati Electrical Low-Pressure Impactor (ELPI+) for particle size distributions and LDSA, the Aethalometer (AE33) and micro Aethalometer

(MA200) for BC, the Partector for LDSA, CO_2 Analyser (LI-840A) and NO_x analyser (T201).

The measurement was done by driving in traffic through the same path multiple times a day while continuously collecting samples through an inlet mounted in the front of the car roof. The route took approximately 12 minutes to complete. At ten predetermined locations in the route a timestamp was logged. These locations were used to determine the start and end of each section of the route and allow us to compare the spatial and temporal variations in particle concentrations. Background measurements for the baseline concentrations of gas and particles were taken in Pyynikki near the Villilänsalmi lake. This allowed us to compare the traffic results with a significantly less polluted location that represents the expected concentrations outside traffic.

The main sources of uncertainty in the study come from the variable number of cars on the road during different days, which influences the measurements but are not normalized for. Since the times are logged manually, human error is also a contributing factor to the uncertainty in the data. Furthermore, instruments have their own internal clocks that are not synchronized. Despite being a constant difference, correcting it manually leads to small but relevant uncertainty in the data. We also do not account for how differences in the weather might have affected particles and gas concentrations.

However, this analysis has the intent of understanding the trends in a large amount of data. With the extensive number of times the route was completed per day and the substantial number of days in which the experiment was conducted, it is possible to draw accurate averages and conclusions. Hence, we were not aiming to analyze a single day or moment, but a trend in gas and particle concentrations and distributions during the lockdown, and how it might be different from circumstances without the lockdown in place.

2. THEORETICAL BACKGROUND

The measurement campaign included diverse types of measurements. The method of gathering and calculating results are explained in detail in this section. These are divided into four categories. Black Carbon, LDSA, Particle concentration and distribution, and CO_2 and NO_x concentrations.

2.1 Black Carbon

Black carbon, sometimes colloquially referred to as soot, is the result of burning fossil fuels at low temperatures. [3] Chemically, BC is the result of an incomplete oxidation of the carbon in fuels and an unnecessary by-product of CO_2 emissions. With the modern interest in mitigating Global Warming, BC is a point of interest since it can embed itself in the snow, thus changing the Earth's albedo and exacerbating the effects of human emissions on the climate. [4] Furthermore, Black Carbon has been linked to respiratory problems [7] and should be considered when discussing public health. However, there is little research linking the effects of particulate matter, including Black Carbon, on individual human health despite the demonstrably negative effect on public health.

Most BC emissions come from road transport [4], therefore a study of road emissions during an abnormal situation such as the pandemic could give us an insight on how a diminished fleet of cars on the road influences the BC concentrations in an urban setting.

The BC mass measurements were taken using the Aethalometer and microAethalometer at different locations and times of day. Both instruments measure BC through optical means.

Emission factors are determined with a ratio between the concentrations (such as BC and particle number) minus their background values and the amount of CO_2 emissions generated by traffic according to equation 1. This allows us to have an estimate of how much mass of Black Carbon is produced by part of CO_2 in the atmosphere.

$$Emission\ Factor = \frac{Measurement - Background}{Measured\ CO_2 - Background\ CO_2} \qquad \textbf{\textit{Eq.1}}$$

Since our instruments measure both CO_2 and NO_2 in PPM and PPB respectively, we must calculate that in terms of mass per volume to compare it to other instruments. To do that we can use the ideal gas law.

$$PV = NRT \qquad \textbf{Eq.2}$$

Where *P* is the pressure, *V* is the volume, *N* is the number of mols, *R* is the idea gas constant and *T* the temperature. Using $R = 8.31\ J{\cdot}K^{-1}{\cdot}mol^{-1}$ for a room temperature of 23 °*C* and pressure of 1 *atm,* we can calculate a gas occupies approximatelly $V = 2.43{\cdot}10^{-2}\ m^3{\cdot}mol^{-1}$. That means that the PPM and PPB concentration will be their respective fraction of that volume. Using the molar mass of CO_2 and the average molar mass of NO (30.01 *g/mol*) and NO_2 (46.01 *g/mol*) with the volume of gass per mol we calculated, we can arrive at the mass of those gasses per meter cubed of air as:

$$Concentration\ CO_2 = \frac{PPM_{CO_2}}{10^6}\frac{N}{V}\frac{M}{N} = \frac{PPB_{CO_2}}{10^6}\frac{M}{V} \qquad \textbf{Eq.3}$$

$$Concentration\ NO_x = \frac{PPB_{NO_x}}{10^9}\frac{N}{V}\frac{M}{N} = \frac{PPB_{NO_x}}{10^9}\frac{M}{V} \qquad \textbf{Eq.4}$$

Where M is the molar mass. We will use 44.01 *g/mol* for CO_2 and 38.01 *g* for NO_x.

2.2 Lung Deposited Surface Area

There is disagreement on the relation between particles smaller than 100 nm, referred to as ultra-fine particles (UFP), and human health, especially in the long term, but the existing studies have been enough to ascertain an increase in all-cause mortality. [8] [9] For this reason, we measured the total LDSA in different environments, as well as particle size distribution. Not much is known about specific direct and indirect health effects of LDSA, but since a correlation has been established, it is important to monitor it and make the data available if we wish to understand its impact in public wellbeing and the environment. To measure LDSA, we used two instruments, the ELPI+ and the Partector.

2.3 Particle Number Concentration and Size Distribution

Fine particles have detrimental effects on human health. Although the mechanism by which this happens is not well understood, the relationship between fine particles and

human health is well established [7] [9]. Particle number concentrations were measured by the CPC and the size distributions by the ELPI+.

2.4 CO_2 and NO_x Concentration

Carbon dioxide is a well-known by-product of the combustion of fossil fuels, and its impact on human health and the climate is well studied. However, NO_x is often overlooked when talking about combustion by products. NO_x is also a common by product of air travel [10], and, due to the impact the COVID-19 lockdowns had on air travel, is an important metric to determine the extent of the pandemic's effect on gas and aerosol concentrations in the atmosphere.

3. FIELD MEASUREMENTS

3.1 Route and Routine

Field measurements were taken during 24th of April and 15th of May in 2020. During this period, a route on the centre of Tampere was established as Figure 1 elucidates.

Figure 1: Map of the route taken by the AtMo-Lab.

Each repetition of the route took approximatelly 12 minutes to complete and was repeated throughout 8am to 4pm with only minor stops during lunch hours, hence a gap in midday measurements. Background measurements, that is, measurements at a sufficiently large distance away from roads so that they are not contaminated by automobile exhaust emmissions, were taken once a day in Pyynikki near the Viilli-länsaumi. Their duration was approximately 5 minutes. Furthermore, zero measurements for the purpose of calibrating and correcting possible offsets in the instruments were done before the start of the day, lunch hours and at the end of the day. Zero measurements are samples taken after being filtered through a High-Efficiency Particulate Air filter (HEPA filter).

The route was divided into ten sections that are referred to as “locations”. These locations are:

- North Tunnel: tunnel road on the North direction
- Paasikiventie: urban road on the west direction
- Stop Light: first stop light
- Motorway: motorway on the west direction

- Roundabout: roundabout and short lakeside road
- Motorway 2: motorway on the east direction
- Stop Light 2: second stop light
- Paasikiventie 2: urban road on the east direction
- South Tunnel: tunnel road on the South direction
- Roundabout 2: roundabout between tunnel drives

License plates were also collected from any car within view. This data, although useful to estimate the fleet of cars in Tampere, will not be used in the analysis presented here.

3.2 Experimental Set up

Figure 2 describes how the instruments were set up during the experiment.

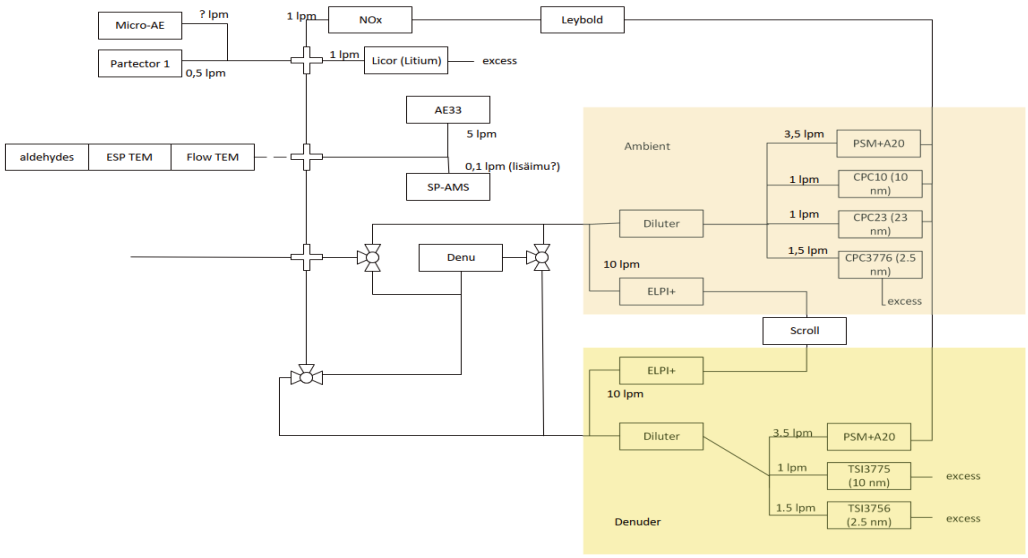

Figure 2: Instrumental set up inside the Atmo-Lab

The inlet was mounted above the car's windshield. For the purposes of this paper, we are analysing the CPC3776 for particle concentrations, the ELPI+ for total mass, particle

distributions and LDSA, the AE33 and MA200 for Black Carbon concentrations and the partector for LDSA.

3.3 Aerosol and Trace Gas Mobile Laboratory

The AtMo-Lab is the laboratory used for this experiment. It is a van equipped with a front facing inlet by which the samples are captured. The instruments are secured on the back of the van and powered by an internal battery. The laboratory can be outfitted as necessary with instruments for a specific measurement campaign.

3.4 Sources of Uncertainty

Before the beginning and at the end of each measurement day, zero measurements were collected using a HEPA filter. This measurement is later used during the data analysis to correct potential errors throughout the day. However, besides the small internal uncertainty in each instrument, the unpredictable nature of the traffic and weather around us adds to the error in each of the measurements.

Traffic is unpredictable and cars passing by near the ATMo-Lab can produce a short spike in particle detection in the instruments, which skews the average toward higher values. To mitigate these errors, the measurements were taken over multiple days and multiple times a day so that no individual car can shift the results significantly. Furthermore, as will be discussed in section 4.1, using a geometric mean across the data ensures us a measurement closer to the peak of the distribution of values than an arithmetic mean.

Another source of error comes from the variations in local weather. The goal of the study is not to understand how alterations of weather affect aerosol emissions in traffic. However, since the measurements were not normalized for those differences, they are a source of error. Once again, we attempted to reduce its impact by taking measurements over a broad number of days to minimize the impact of variations in temperature, humidity, atmospheric pressure, etc...

The final error source to consider is the time delay between instruments receiving the sample from the inlet. We also need to consider how, due to human error, small differences in the timing of each timestamp are possible. Those errors were corrected manually by observing the data in a single instrument and observing the first measurement of the day (North Tunnel) and last measurement of the day (South Tunnel), both of which produce peaks in particle detection. The raw data is then shifted timewise uniformly until

the first and last peaks of the day fit within the boundaries. This kind of correction was done for every day and every measurement used in this study.

Figure 3 is one example of raw data from one of the days of the measurement campaign. The blue and yellow lines represent the *fA* currents captured by the ELPI+. The black lines represent the time boundaries of the tunnel measurement. The graph on the left has some of the peak is outside the boundary of the tunnel and this does not represent what the field team observed while in the ATMo-Lab. The graph on the right shows the raw currents after being corrected. The two peaks are better constrained within the black lines and better represent the reality of the measurement.

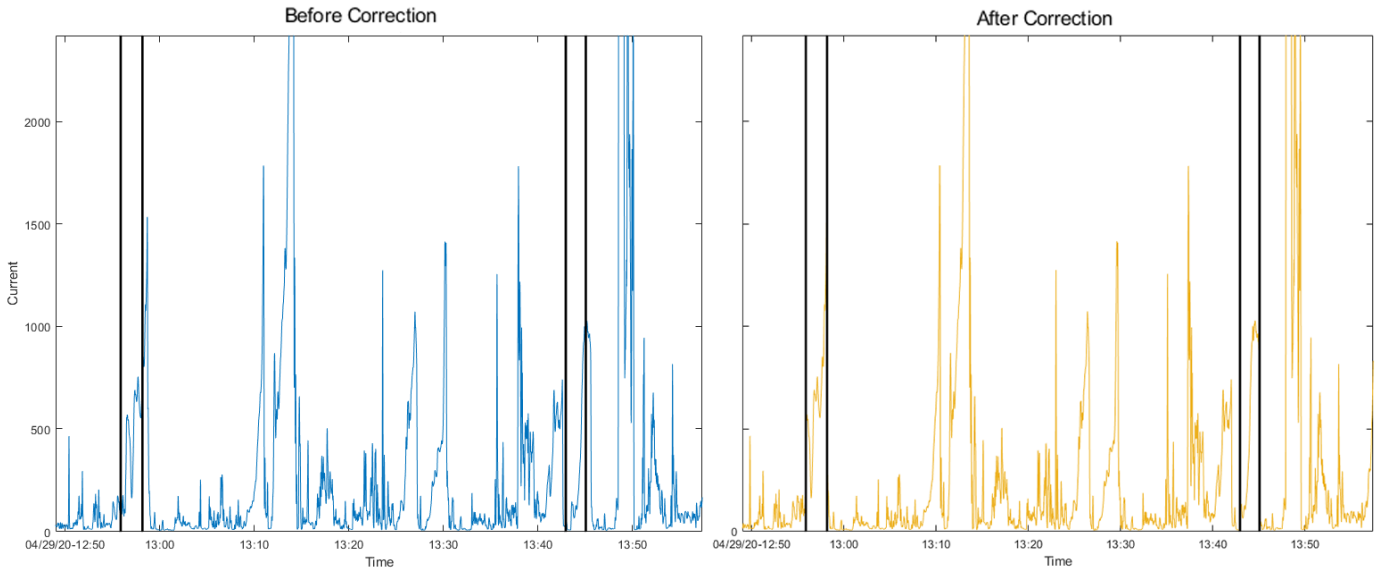

Figure 3: Example of pre and post-correction raw data from the 3rd impactor of the ELPI+ in the first day of measurements.

4. DATA ANALYSIS

The data collected was extensive with some instruments crossing over three hundred thousand individual data points. This data needs to be corrected, split, and averaged. The study focuses mostly on the location in the route, but we were also interested in the evolution of values throughout the day.

Raw raw data was time corrected and then separated into each of the ten locations according to the moment it was measured. With the data sorted into locations, two types of analysis were done: by location and by time. Analysis by location was done by averaging all the 1 second data points collected during the whole period of the experiment in that specific location. Time measurements were done with a similar method, but instead of dividing the measurements in a specified location, all the data that was collected within a certain time boundary was averaged.

4.1 Method of Averaging

The instruments used during measurements save data at *1Hz*. With our interest in averages and general trends of individual locations, and not in transcendental data, we must choose an appropriate method of averaging for the upwards of two hundred data points we collected in some locations.

After comparing values and errors from arithmetic and geometric averages, we chose to use geometric means. Since the distribution of measurements is wide due to e.g., large vehicles driving close to the inlet tube, an arithmetic did not produce values that we considered to correspond with the reality of the data. Geometric means, on the other hand,

give us a value closer to the peak of the distribution. Figure 4 shows the difference between averages by plotting the distributions of all BC values measure in the North tunnel.

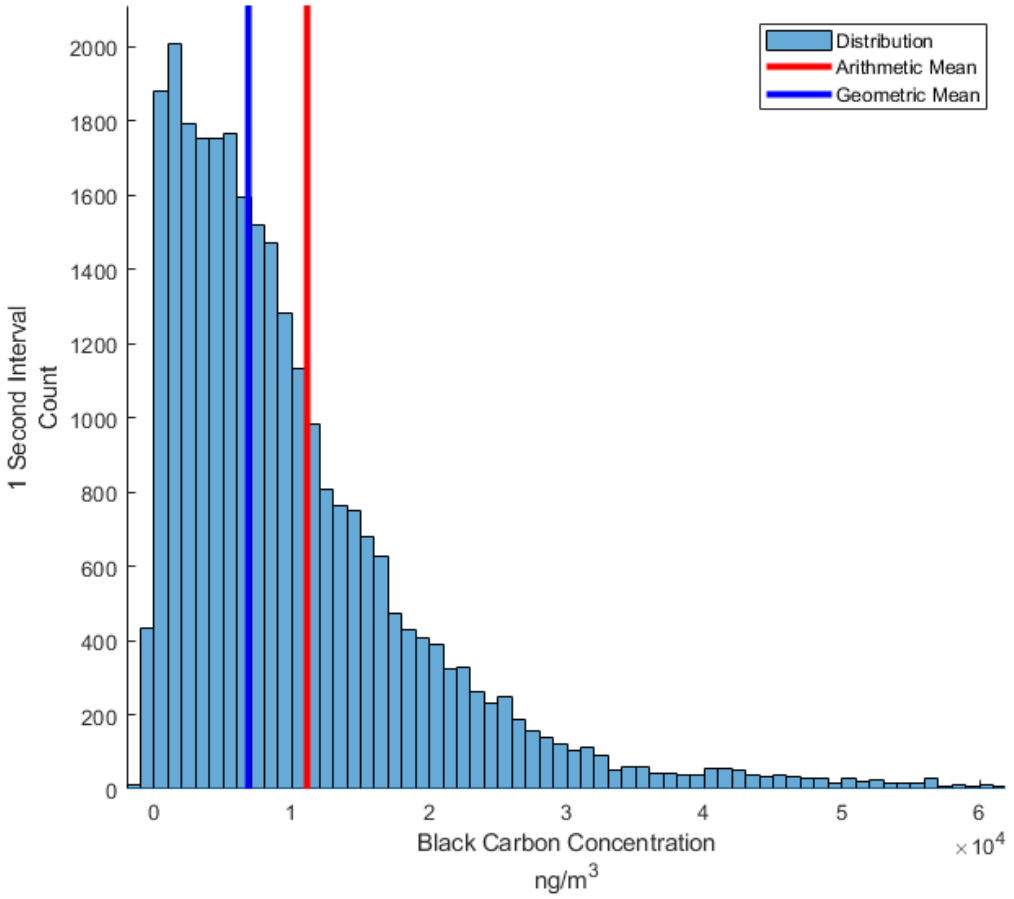

Figure 4: Comparison between Arithmetic and Geometric averaging methods for Black Carbon value distribution

This decision was done since we have a broad spectrum of measurements during all days and locations, so it becomes complicated to compare them with a simple average. However, if we understand that the measurement, we are looking for is the one that a

random sample of the environment would contain. For this reason, the peak of the distribution of values is of interest. Geometric means ensure that the relatively rare large measurements do not skew the data as far as an arithmetic average would.

To ensure the data is comparable between instruments, geometric means have been used for all averages.

4.2 Black Carbon

Black carbon was measured using the MA200 and the AE33. The MA200 recorded over 100000 instances of measurements and the AE33 over 300000. Since both BC instruments measure the values in ng/m^3, no more treatment is needed to ensure the data is meaningful and comparable.

4.3 Particle Number Distribution and Size Concentrations

Particle distributions were measured using the ELPI+. The ATMo-Lab had one ELPI+ measuring aerosol size distributions. The ELPI+ works by receiving particles through an inlet. The particles pass through the charger stage where they receive a small amount of charge. After that, they move into the impactor stages wherein they will either hit the detector plate or, depending on their momentum, move to the next stage of detection. When a particle hits one of the detector plates, its charge is detected and measured in fA.

The data is recorded in fA and converted into a distribution using a coefficient matrix [11] and collection efficiency [12]**.** Furthermore, we correct for diffusion (that is, the possibility of particles being detected in the incorrect stage of the ELPI+ impactor). This data is then used to calculate total mass and particle concentrations.

The data is displayed as *dN/dlogdp,* a lognormal distribution since they are the best fit for the data. *N* is the number of particles and *dp* the particle diameter. The reason for the

use of this method is entirely empirical since aerosol distributions fit well into a bell curve when using this lognormal distribution [13].

Furthermore, we used a CPC to measure the particle number concentrations. The CPC used is also referred to as CPC56 for its model number and has a cut off size of 2.5 nm. The instrument works by enlarging the particles with butanol and measuring it optically.

4.4 Lung Deposition Surface Area

The LDSA was measured using two instruments. The first of which is the ELPI+. The instrument collects data in the form of fA. This data is then converted into LDSA through coefficients. The process works similarly to the particle distribution calculations. [11].

The second instrument is the Partector, which gives us direct readings in $\mu m^2/cm^3$. It is important to note that during the experiments, the values of the Partector followed closely with the ELPI+ values, but at a 2.7748 times smaller result on average. This leads us to believe there is some source of systematic uncertainty in the instrument, such as losses or a diameter-based cut-off point in detection of particles. Another possible explanation is the fact that the Partector assumes a baseline distribution for the particles while the ELPI+ can give us the current distribution. For this reason, the Partector data was not included in this thesis and will not be taken into consideration for any conclusions drawn from the data.

LDSA measurements are divided in three different areas: “Alveolar” accounts for the deposition in alveoli in the lungs, “Tracheobronchial” for the deposition in the trachea and bronchi, and “Head” for the deposition in the head airways. The “Total” value is the sum of all previously mentioned depositions.

The physical quantity for the deposition is calculated primarily in $\mu m^2/cm^3$, that is, the expected area of deposition in micrometers through the inhalation of a volume of air in centimeters cubed.

4.5 Gas Concentrations

NO_x and CO_2 were both measured throughout the campaign. The instruments used were T201 and the LI-840A respectively. The values were time corrected to be in sync with the other instruments and then averaged geometrically. CO_2 is measured in PPM by the

instrument itself, while NO_x is measured in currents and converted into PPB by a factor of 1.838 according to the last calibration of the instrument by the Aerosol Laboratory.

4.6 Emission Factors

Emission factors are a good form to interpret the results from the previous data that allows us to compare the data with other studies. With it, we can estimate the number of aerosols created based on the amount of CO_2 produced in a car. For these measurements, we have calculated the ratio of Black Carbon mass and CO2 over the background level.

5. RESULTS

5.1 Particle Distributions and Concentrations

Particle distributions and concentrations are measured by the ELPI+ and the CPC53 respectively. It is expected to see a correlation between data in both since the ELPI+'s distribution, ideally, has the same number of particles in total as a sample measured by the CPC53. Differences can be attributed to different cut off points in particle diameter for each instrument.

5.1.1 Particle Distributions

The particle size distributions per location were calculated using the ELPI+. In Figure 10, the sizes in the x axis are the cut off points for each one of the impactors.

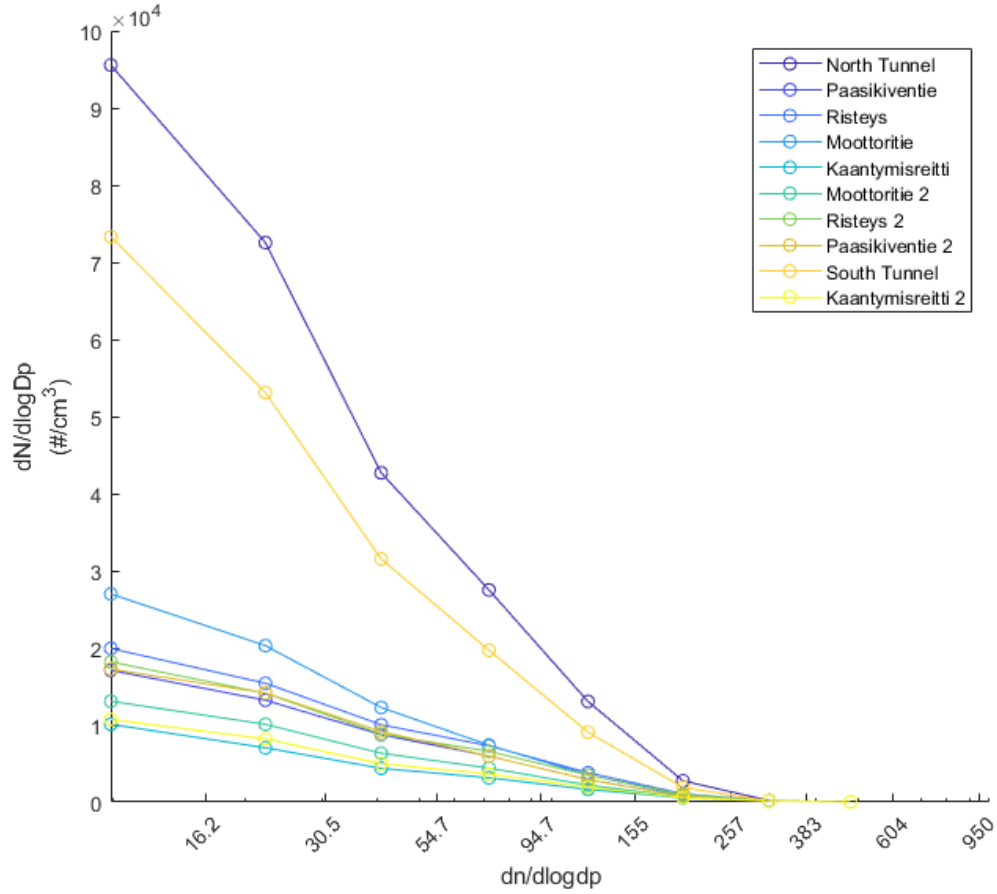

Figure 5: Particle size distribution measured by the ELPI+

Here we can see the clear trend of distribution that both tunnels follow. Values of *dn/dlogdp* were cut off starting from 481 since the values are too small to be visible in

this graph. The full list of values is available in Table 5 in Appendix A. The cut off points for each impactor are also described in meters and available in Table 4 in Appendix A. Please note the detection counts are still displayed as *dn/dlogdp*.

5.1.2 Particle Number Concentrations

Particle concentrations were measured by the CPC56. In Figure 11 we can see the expected result wherein North and South tunnels have the highest concentration of particles.

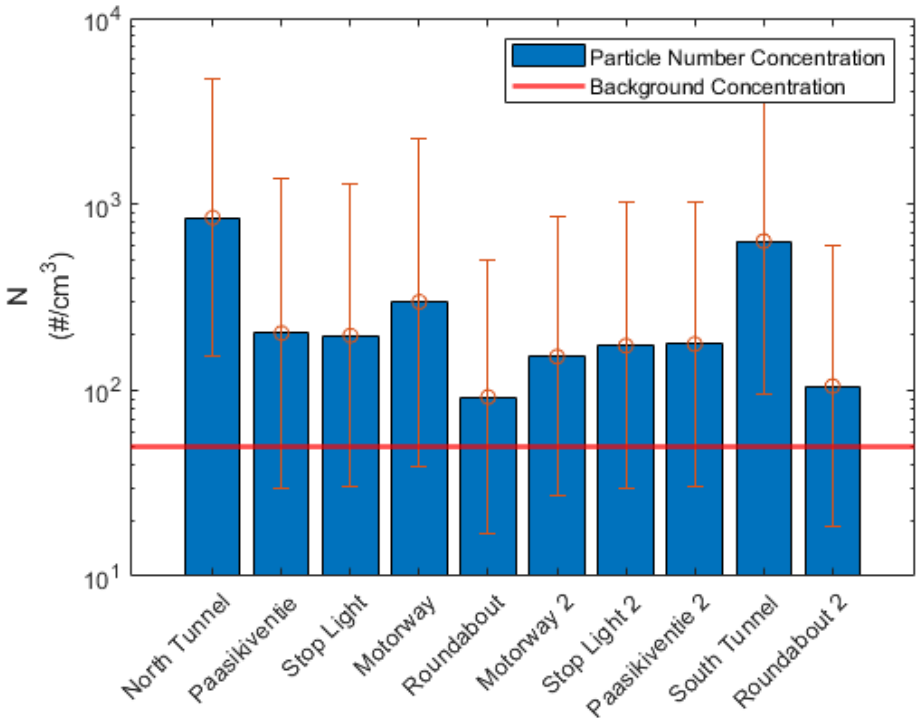

Figure 6: CPC56 particle concentration geometric mean according to location

These measurements will be used further in the emission factor discussion in the next subchapter.

5.2 Black Carbon and LDSA

Black carbon and LDSA were closely correlated during the measurements. For this reason, it is important that we evaluate both individually and together to understand their connection and evaluate the accuracy of our measurements.

5.2.1 Black Carbon

Looking at the concentrations averaged by location from the Black Carbon, we have the highest concentrations in the two tunnels as expected. The difference in the values of

the North and South tunnel can be attributed to the direction of the flow of traffic during the experiment's schedule. Figure 5 displays the geometric mean of black carbon across all locations by the Aethalometer. Each average is comprised of all measurements taken within the boundaries of the location throughout the entirety of the measurement campaign.

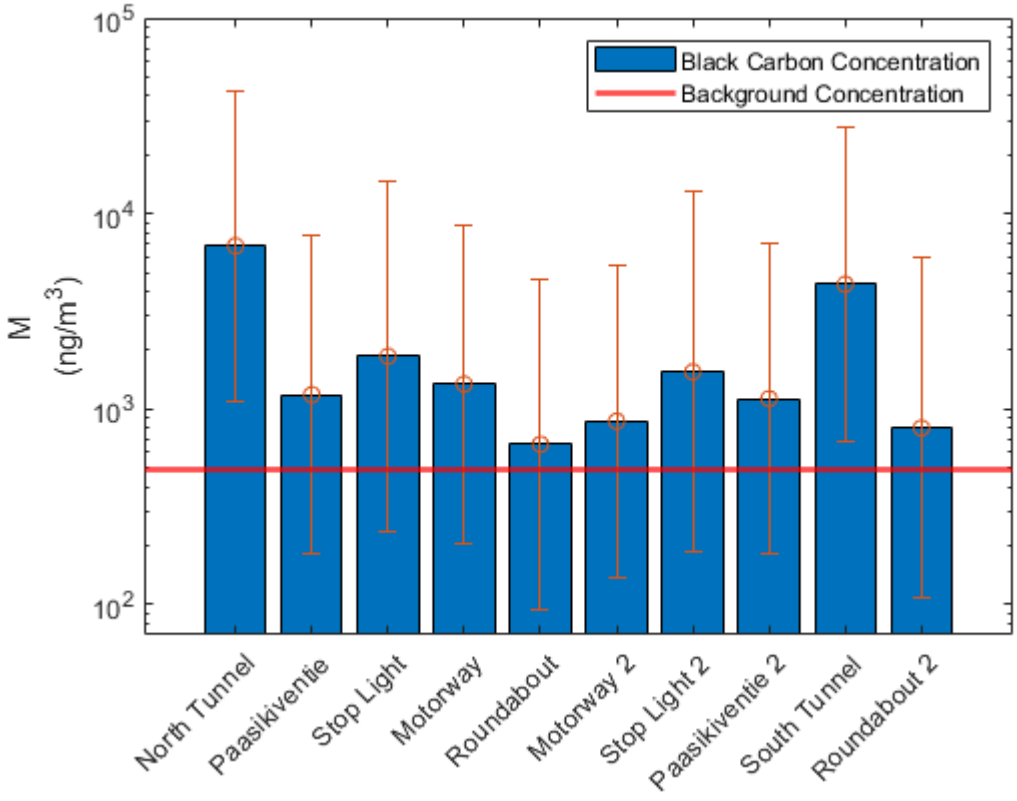

Figure 7: Black Carbon geometric average by location measured by the Aethalometer (AE33)

In comparison, we have the same measurements from the microAethalometer. The same trend can be seen in the measured values as the Aethalometer; however, the values are significantly higher. Figure 6 displays the results of the geometric mean of all measurements divided by location as measured by the microAethalometer.

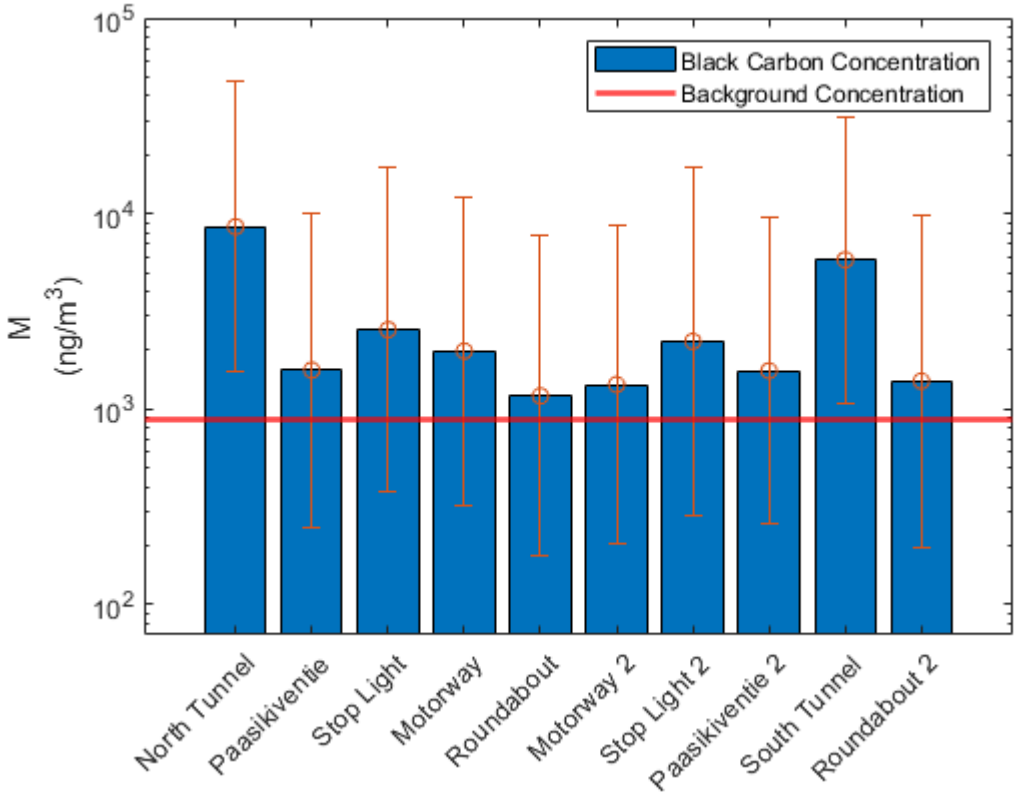

Figure 8: Black Carbon geometric average by location measured by the microAethalometer (MA200)

For a more specific numeric comparison, we have Table 2 in Appendix A. The differences in uncertainty and values can be attributed to the different methods of measurement in the instruments. For further comparison, Appendix A contains the tables with the values and errors.

The high value for the geometric STD of the order of 3 is expected considering the number of variables in the measurements such as number of vehicles, density of traffic and models. However, the similar values are a good indication that the effects of this randomness are uniform across different measurement locations. Also note that these values are only for the Aethalometer.

We can also look at temporal variations in BC concentration in a fixed location. Note that the measurements labelled as “8am” encompass the time between 8:00 to 8:59. The

same standard is used for all other times in the measurement. The following measurements only consider the measurements from the Aethalometer, not the microAethalometer.

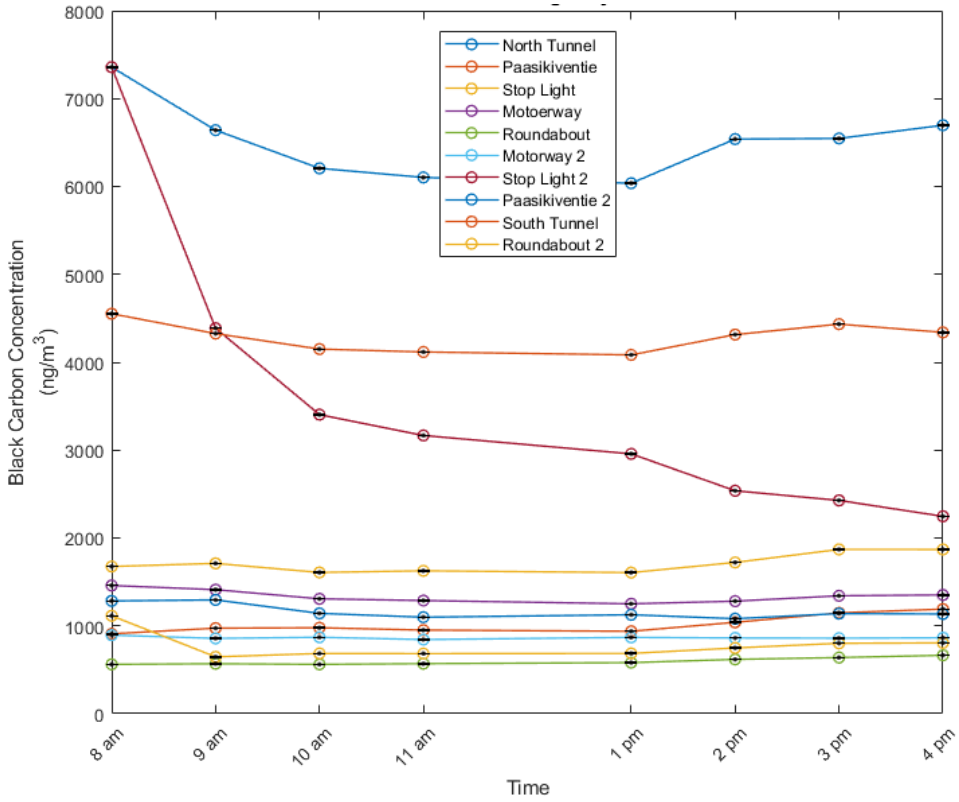

Figure 9: Black Carbon geometric average concentration values evolution through the day measured by the Aethalometer (AE33)

Most notably, Risteys 2 has a substantially higher peak at the beginning of the day. Since Risteys 2 is one of the traffic stops in the measurement route, we can assume the large change is due to the flow of traffic during early morning, when most people are driving to work. We can speculate that measurements after 4pm during the second rush hour of the day could show us a similar increase in the concentration of BC in other locations, but we lack the data to affirm that for sure. A future experiment could gather data at

different times to broaden our understanding of the evolution of concentration of BC in roads throughout the day.

5.2.2 Lung Deposition Surface Area

The LDSA results closely resemble the BC. This will be discussed further in the next part of the thesis. The North and South tunnels have the highest overall concentrations while the other locations remain relatively similar to each other.

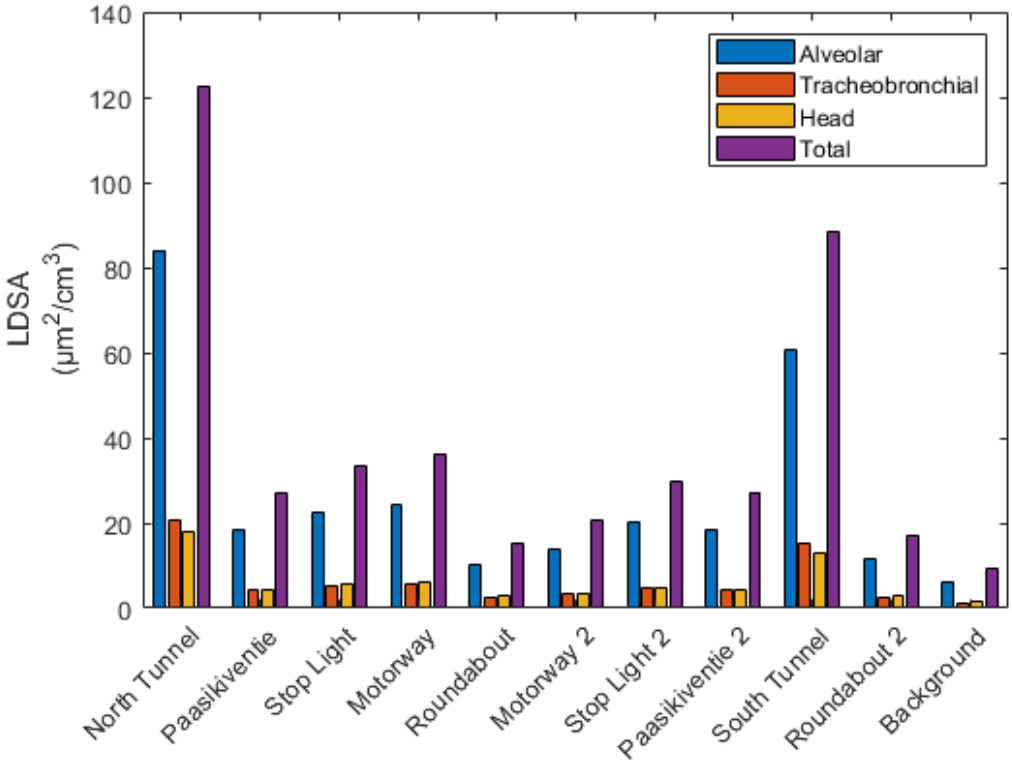

Figure 10: Lung Surface Deposition Coefficient (LDSA) Average by Location measured by the ELPI+

Table 3 in Appendix A has the results in more accurate numbers including the total LDSA for each location. These results were measured by the ELPI+ only and do not take into account any data gathered by the Partector.

5.2.3 Comparison Between LDSA and Black Carbon

LDSA and BC follow a close trend together. The graphs in figure 9 exemplify this correlation according to each location and time. The values used for this analysis were all the data points that conformed to the location and time throughout the entirety of the

measurement campaign. Only the North and South tunnel are displayed in Figure 9. The other locations can be found in Appendix B.

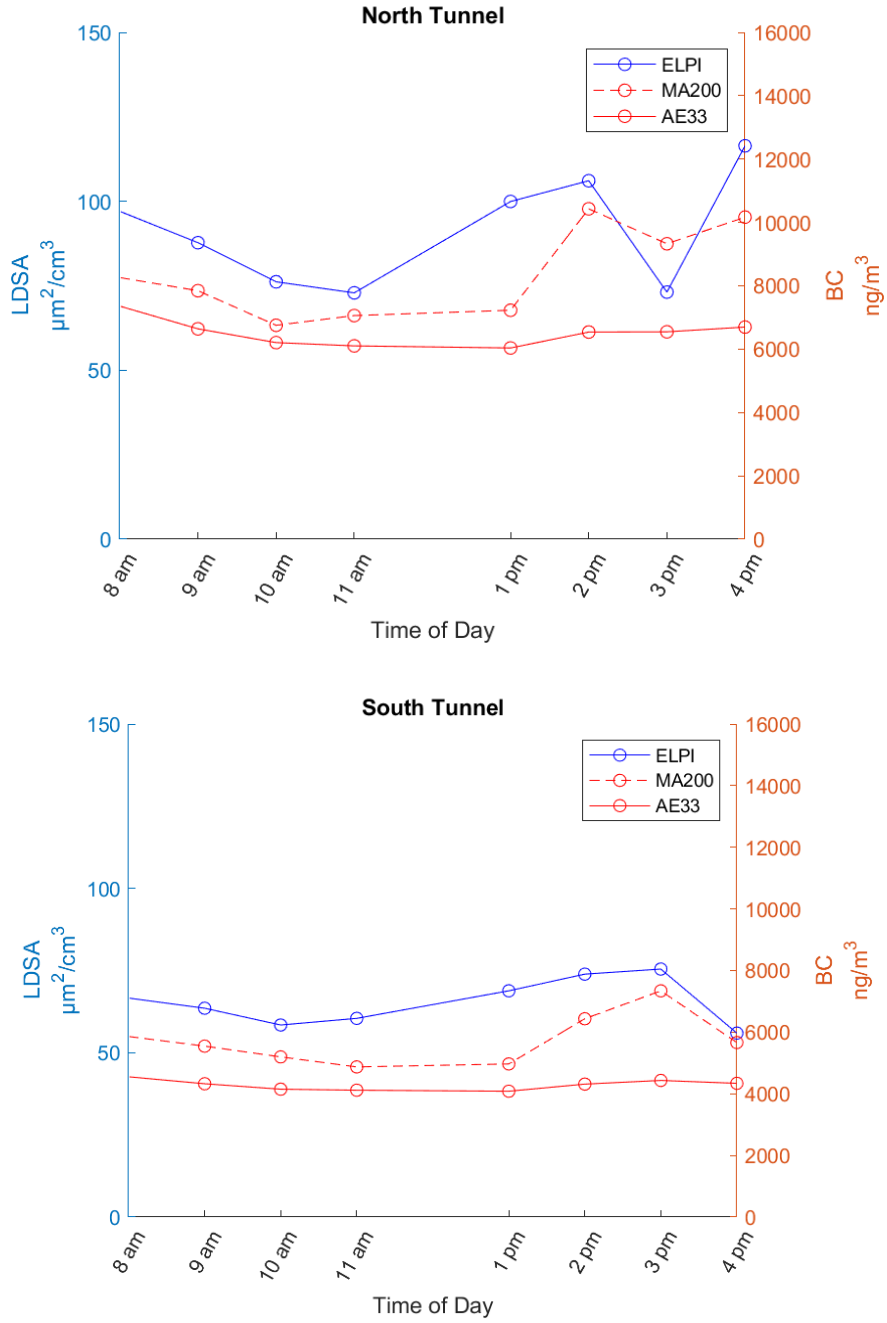

Figure 11: LDSA and Black Carbon in the North and South tunnel. Evolution of concentration is shown throughout the day. Averaged geometrically

5.3 Gases and Emission Factors

From these measurements we can gain good insight of how many particles we expect to be produced by each part of a gas above the baseline. In these measurements, we use CO_2 as the gas since it is the expected product of fossil fuel combustion in engines.

5.3.1 Gas Concentrations

The gas concentrations are the first step to calculate the emission factors. From Figure 12 we can see that some of the less busy locations in the measurement give us lower CO2 concentrations than the background locations. That is most likely due to the large uncertainty in the measurements.

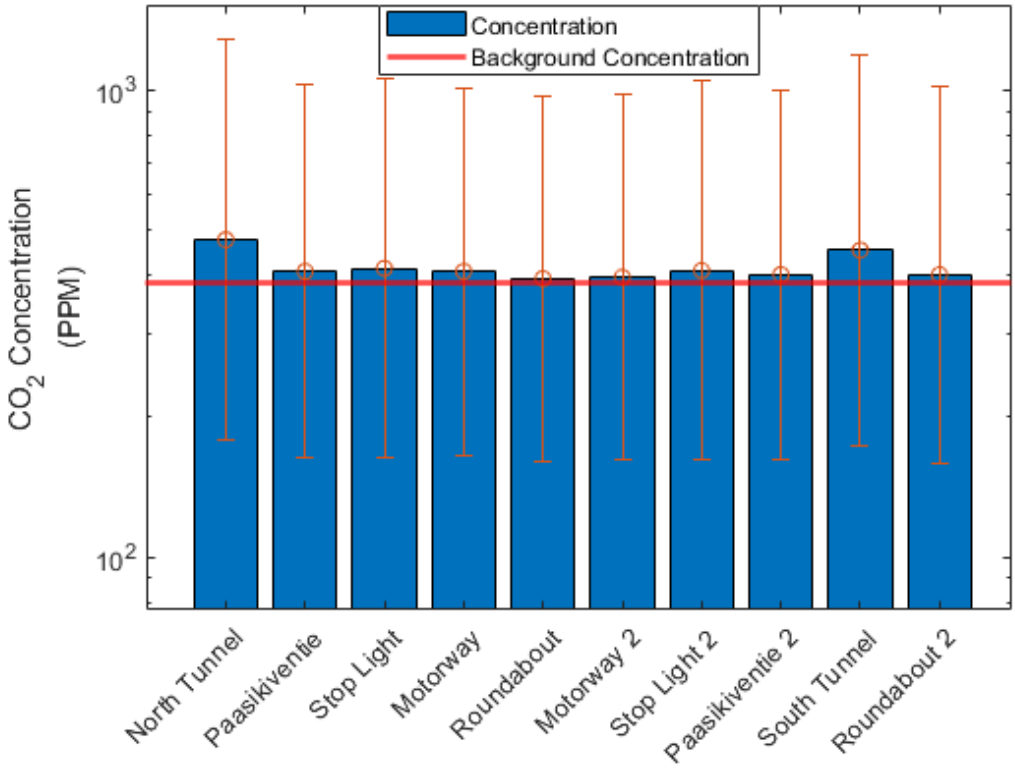

Figure 12: CO_2 concentrations geometric mean according to location. The red line is the CO_2 measured in the background locations.

The same trend can be observed in the NO_x results which are displayed on Figure 13, which points to a systemical uncertainty source.

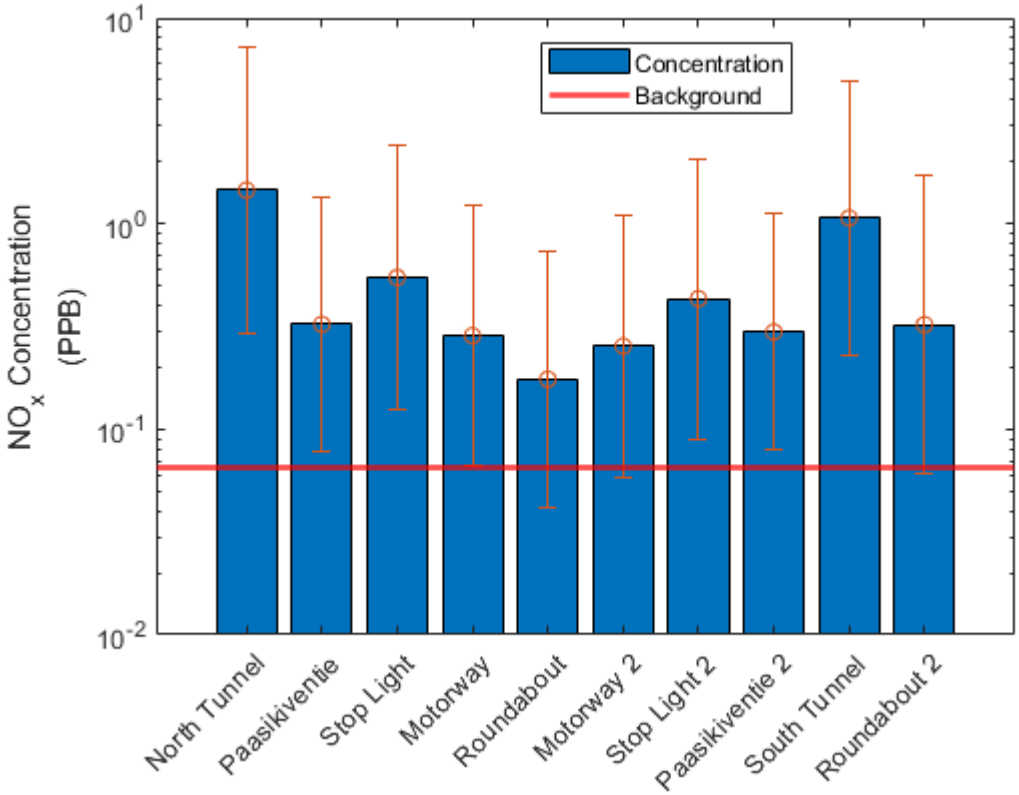

Figure 13: NOx measurements geometric mean based on location. The red line is the background location NOx concentration.

Numeric information about the CO_2 and NO_2 concentrations and their respective geometric standard deviations can be found in Appendinx A in Table 7.

5.3.2 Mass Concentration

Total mass is measured by the ELPI+ as currents and gives us an estimative of the total mass of particles in a certain volume. Figure 14 is the plot of the geometric average of the total mass in each of the locations. Using different cut off points, we can see that in the North and South tunnel most of the mass comes from particles below 2.5 μm and

above 1.0 µm threshholds. It is also important to note that very little of the total weight comes from particles between 0.5 µm and 1 µm.

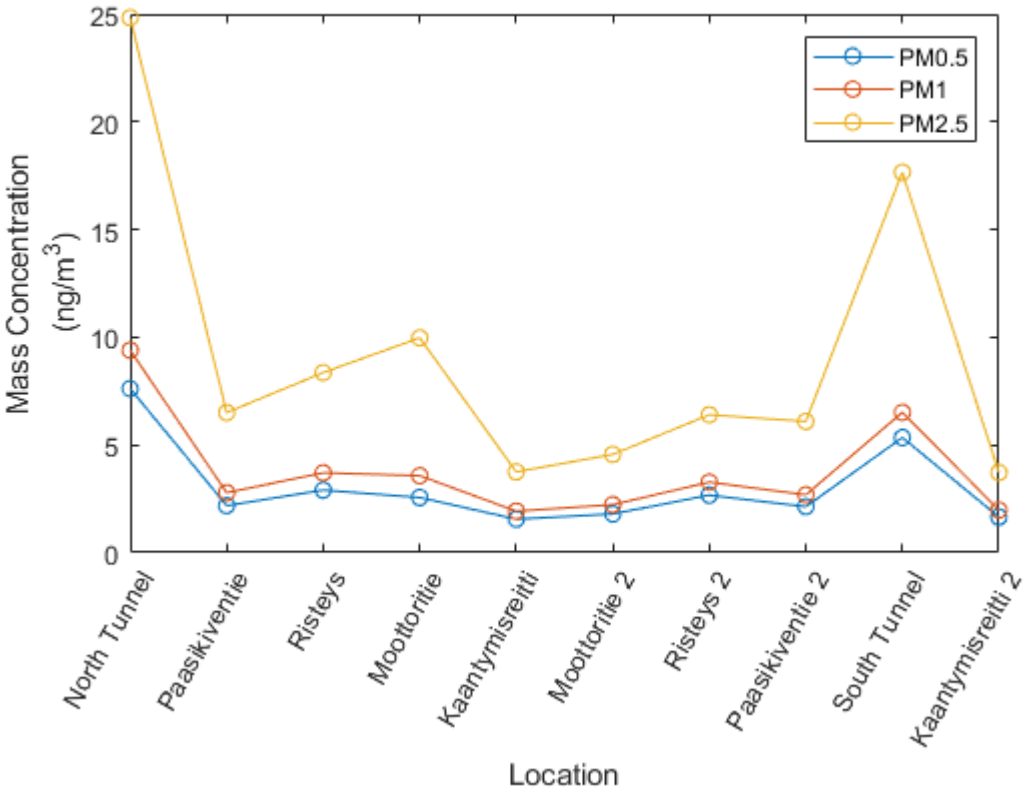

Figure 14: Total mass of particles at different cut off points measured by the ELPI+

It is important to note that PM2.5 is not the most reliable measurement since it accounts for larger particles. Small uncertainties in the count of those particles have a large impact in the total mass.

5.3.3 Emission Factors

These measurements will attempt to determine the average number of particles, the total mass and the NOx related to each PPM of CO2 released into the atmosphere by automobile exhausts in Tampere. This number does not account for vehicle types and is not normalized for variations in climate.

Most of the locations have concentrations of gasses only slightly above the background level. This can be accounted due to the large uncertainty in the measurements and, as a result, leads us to physically meaningless results such as negative emission. For this

reason, only the North and South Tunnel locations will be used to calculate the emission factors.

Table 1: Emission factors for North and South Tunnel

Location	North Tunnel	South Tunnel
Total Mass PM0.5 (mg/mg CO_2)	$3.88 \cdot 10^{-03}$	$3.40 \cdot 10^{-03}$
Total mass PM1.0 (mg/mg CO_2)	$4.88 \cdot 10^{-03}$	$4.25 \cdot 10^{-03}$
Total Mass PM2.5 (mg/mg CO_2)	$1.38 \cdot 10^{-02}$	$1.29 \cdot 10^{-02}$
Black Carbon (mg/mg CO_2)	$3.80 \cdot 10^{-03}$	$3.12 \cdot 10^{-03}$
Particle Concentration (#/mg CO_2)	$4.77 \cdot 10^{-01}$	$4.71 \cdot 10^{-01}$
NO_x (mg/mg CO_2)	$7.87 \cdot 10^{-03}$	$7.53 \cdot 10^{-03}$

6. CONCLUSION

The measurement campaign in Central Tampere during the COVID-19 lockdown gives us good insight on the values of the black carbon around central Tampere. While 8 out of the 10 locations measured have given us values comparable with the background concentrations of BC, LDSA and particles, the North and South Tunnel give us a better look at the Emission Factors. Despite the high variance, the consistency of values between North and South tunnel are a good sign that we have an accurate idea of particle emissions according to CO2 emissions in Tampere. Looking at the evolution of values throughout the day, only Stop Light 2 distinguished itself from other values by having a significantly higher concentration of particles early in the morning. Other locations have shown to retain the same constant value throughout the day.

The background values of 0.48 $\mu g/m^3$ of Black Carbon in Tampere are below that of large cities like New York, where the background values vary from as low as 0.23 $\mu g/m^3$ to 7.67 $\mu g/m^3$ [14], and São Paulo where values averaged around 10.5 $\mu g/m^3$ [15]. However, in the North and South tunnel we have observed averages of of 6.83 $\mu g/m^3$ and 4.35 $\mu g/m^3$. Commuters in Tampere are exposed to large concentrations of Black Carbon during their routes. Considering the impact of Black Carbon on public health, it might be worthy of consideration to improve ventilation in tunnels, especially those that are in commuter routes.

Furthermore, we have found the Partector to be somewhat unreliable when compared to other robust instruments such as the ELPI+. For qualitative analysis, the Partector is appropriate, but its results in the quantitative analysis are dubious and should be compared to other instruments before being used.

The broad distribution of the data complicates the analysis, increasing the variance, which adds uncertainty to any assumptions that we attempt to make with simple averages. This is as expected since there are far too many variables that cannot be controller for when taking measurements, such as traffic and climate. However, the consistent geometric standard deviation points to a constant randomness, which allows us to make comparisons between instruments and values.

The values found in Table 1 can be used for modelling car emissions in central Tampere based on the amount of emission from car exhausts. Further modelling of trends and distributions would require a more comprehensive analysis of the trends in this data, but

we are confident that the emission factors are a good representations of car exhaust emissions of the fleet of cars in Tampere on average.

Comparison of this data with other real time statistics is complex since adding more variables makes any comparisons dubious. We propose that a similar study be done after the COVID-19 lockdown situation normalizes and regular traffic is resumed using the same route in this campaign. This study and the available data can be used as a point of comparison to further analyse the extent of the COVID-19 pandemic effect on automobile exhaust emissions and, perhaps, draw additional conclusions about the effects of traffic on these measurements. There is also data from this study that has not been used in the analysis, such as the collection of license plate numbers collected during measurement. They could, in the future, be utilized to estimate the composition of the fleet of cars in Tampere.

REFERENCES

[1] C. Arden Pope III, R. T. Burnett ja M. J. Thun et al., ”Lung Cancer, Cardiopulmonary Mortality, and Long-term Exposure to Fine Particulate Air Pollution,” *JAMA,* p. 287(9):1132–1141, 2002.

[2] O. Boucher ja D. Randall et al., ”AR5 Climate Change 2013: The Physical Science Basis Chapter 7: Clouds and Aerosols,” IPCC, 2013.

[3] A. P. Voiland, ”Black Carbon: A Global Presence,” 9 August 2011. [Online]. Available: https://svs.gsfc.nasa.gov/3844.

[4] T. C. Bond ja H. Sun, ”Can Reducing Black Carbon Emissions Counteract Global Warming?,” tekijä: *Environmental Science & Technology*, American Chemical Society, 2005, p. 5921–5926.

[5] F. Karagulian, C. A. Belis, C. F. C. Dora, A. M. Prüss-Ustün, S. Bonjour, H. Adair-Rohani ja M. Amann, ”Contributions to cities' ambient particulate matter (PM): A systematic review of local source contributions at global level,” *Atmospheric Environment,* osa/vuosik. Volume 120, pp. 475-483, 2015.

[6] A. Riuttanen , V. Ponkilainen, I. Kuitunen, A. Reito, S. Joonas ja V. M. Mattila, ”Severely injured patients do not disappear in a pandemic: Incidence and characteristics of severe injuries during COVID-19 lockdown in Finland,” 2021.

[7] W. Lin, W. Huang, T. Zhu, M. Hu, B. Brunekreef, Y. Zhang, X. Liu, H. Cheng, U. Gehring, C. Li ja X. Tang, ”Acute Respiratory Inflammation in Children and Black Carbon in Ambient Air before and during the 2008 Beijing Olympics,” *Environmental Health Perspectives,* 1 October 2011.

[8] G. Hoek ja H. Boogaard et al., ”Concentration Response Functions for Ultrafine Particles and All-Cause Mortality and Hospital Admissions: Results of a European Expert Panel Elicitation,” *American Chemical Societ,* p. 476–482, 3 December 2010.

[9] N. Englert ja N. Englert, ”Fine particles and human health—a review of epidemiological studies,” *Toxicology Letters,* osa/vuosik. Volume 149, nro Issues 1–3, pp. 235-242, 2004.

[10] ”EASA,” [Online]. Available: https://www.easa.europa.eu/eaer/topics/technology-and-design/aircraft-engine-emissions. [Haettu January 2021].

[11] M. Moisio, *elpiPlusDiffusionCorrection.m,* 2017, pp. 41-48.

[12] Jarvinen et al., 2004.

[13] TSI Incorporated, *Aerosol Statistics Lognormal Distribution and dN/dlogDp.*

[14] P. Venkatachari, L. Zhou, P. K. Hopke, D. Felton, O. V. Rattigan, J. J. Schwab ja K. L. Demerjian, ”Spatial and temporal variability of black carbon in New York City,” osa/vuosik. 111, nro D10, 2006.

[15] J. Chu, ”Estudo do Impacto do Material Particulado e Black Carbon, na Incidência de Doenças do Aparelho Respiratório em São Paulo,” Universidade de São Paulo, Instituto de Astronomia, Geofísica e Ciencias Atmosféricas, Sao Paulo, 2018.

[16] F. Moisy, *errorbarlog.m,* MATLAB Central File Exchange, 2021.

APPENDIX A: TABLES

Table 2: Black Carbon geometric average and STD by location measured by the AE33 and MA200

Location	AE33 BC (µg/m3)	AE33 Geometric STD	MA200 BC (µg/m3)	MA200 Geometric STD
North Tunnel	6.8296	3.0238	8.5625	2.6550
Paasikiventie	1.1822	3.1732	1.5800	3.1327
Risteys	1.8619	3.8601	2.5470	3.3351
Moottoritie	1.3406	3.1999	1.9787	3.0122
Kaantymisreitti	0.6597	3.4037	1.1658	3.2313
Moottoritie 2	0.8650	3.0883	1.3339	3.1985
Risteys 2	1.5484	4.0956	2.2175	3.8125
Paasikiventie 2	1.1298	3.0517	1.5706	2.9467
South Tunnel	4.3453	3.0984	5.7961	2.6108
Kaantymisreitti	0.7987	3.6401	1.3900	3.4654
Background	0.4864	2.9391	0.8826	2.8017

Table 3: LDSA measured by the ELPI+ by region and totals

	LDSA $\mu m^2/cm^3$			
Location	**Alveolar**	**Tracheobronchial**	**Head**	**Total**
North Tunnel	84.00	20.70	17.93	122.62
Paasikiventie	18.24	4.26	4.44	26.94
Risteys	22.42	5.15	5.65	33.22
Moottoritie	24.22	5.87	6.06	36.14
Kaantymisreitti	10.27	2.34	2.79	15.40
Moottoritie 2	13.81	3.21	3.45	20.46
Risteys 2	20.20	4.64	5.00	29.84
Paasikiventie 2	18.51	4.35	4.40	27.27
South Tunnel	60.59	15.08	12.81	88.48
Kaantymisreitti	11.56	2.65	2.94	17.15
Background	6.26	1.36	1.66	9.27

Table 4: Particle cut off points for each of the impactors. They are displayed in meters

Bin	Minimum Size (m)	Maximum Size (m)
1	6.00E-09	1.62E-08
2	1.62E-08	3.05E-08
3	3.05E-08	5.47E-08
4	5.47E-08	9.47E-08
5	9.47E-08	1.55E-07
6	1.55E-07	2.57E-07
7	2.57E-07	3.83E-07
8	3.83E-07	6.04E-07
9	6.04E-07	9.50E-07
10	9.50E-07	1.63E-06
11	1.63E-06	2.48E-06
12	2.48E-06	3.66E-06
13	3.66E-06	5.38E-06
14	5.38E-06	9.91E-06

Table 5: dNdlogdp averaged geometrically by locations and divided beween each of the ELPI+ impactor cutoffs. These measurements have been corrected for diffusion.

Location	1	2	3	4	5
North Tunnel	9.56E+04	7.25E+04	4.27E+04	2.75E+04	1.30E+04
Paasikiventie	1.71E+04	1.32E+04	8.74E+03	5.97E+03	2.92E+03
Risteys	1.99E+04	1.54E+04	1.00E+04	7.30E+03	3.82E+03
Moottoritie	2.70E+04	2.03E+04	1.23E+04	7.38E+03	3.51E+03
Kaantymisreitti	1.01E+04	7.04E+03	4.38E+03	3.15E+03	1.64E+03
Moottoritie 2	1.31E+04	1.01E+04	6.34E+03	4.41E+03	2.21E+03
Risteys 2	1.82E+04	1.41E+04	8.82E+03	6.58E+03	3.50E+03
Paasikiventie 2	1.72E+04	1.42E+04	9.15E+03	5.98E+03	2.90E+03
South Tunnel	7.33E+04	5.31E+04	3.15E+04	1.97E+04	9.07E+03
Kaantymisreitti	1.07E+04	8.19E+03	4.98E+03	3.64E+03	1.93E+03

Location	6	7	8	9	10
North Tunnel	2.76E+03	2.02E+02	3.02E+01	2.60E+01	1.91E+01
Paasikiventie	7.73E+02	1.34E+02	2.31E+01	8.41E+00	4.58E+00
Risteys	1.08E+03	1.85E+02	3.03E+01	1.15E+01	5.80E+00
Moottoritie	8.74E+02	1.41E+02	2.92E+01	1.48E+01	8.61E+00

Kaantymisreitti	5.50E+02	1.40E+02	2.03E+01	4.84E+00	2.21E+00
Moottoritie 2	6.41E+02	1.31E+02	1.98E+01	5.84E+00	2.90E+00
Risteys 2	9.88E+02	1.75E+02	2.74E+01	8.32E+00	4.04E+00
Paasikiventie 2	7.52E+02	1.27E+02	2.10E+01	7.70E+00	4.14E+00
South Tunnel	1.89E+03	1.45E+02	2.26E+01	1.63E+01	1.32E+01
Kaantymisreitti	5.94E+02	1.33E+02	1.92E+01	4.04E+00	2.03E+00

Location	**11**	**12**	**13**	**14**
North Tunnel	1.40E+01	5.28E+00	1.52E+00	5.93E-01
Paasikiventie	3.15E+00	1.78E+00	1.01E+00	4.62E-01
Risteys	3.85E+00	2.36E+00	1.37E+00	7.07E-01
Moottoritie	5.38E+00	2.71E+00	1.28E+00	5.61E-01
Kaantymisreitti	1.52E+00	9.30E-01	5.79E-01	2.44E-01
Moottoritie 2	1.95E+00	1.14E+00	6.77E-01	2.95E-01
Risteys 2	2.55E+00	1.59E+00	1.14E+00	5.52E-01
Paasikiventie 2	2.91E+00	1.61E+00	8.77E-01	4.29E-01
South Tunnel	1.02E+01	4.15E+00	1.09E+00	4.45E-01
Kaantymisreitti	1.50E+00	8.45E-01	5.45E-01	1.96E-01

Table 6: Total mass by location at three cut off points. Data averaged geometrically and measured by the ELPI+

Location	**PM0.5**	**PM1**	**PM2.5**
North Tunnel	7.615	9.398	24.832
Paasikiventie	2.184	2.785	6.502
Risteys	2.905	3.707	8.361
Moottoritie	2.561	3.573	9.972
Kaantymisreitti	1.555	1.926	3.750
Moottoritie 2	1.799	2.229	4.562
Risteys 2	2.669	3.275	6.402
Paasikiventie 2	2.136	2.684	6.093
South Tunnel	5.344	6.513	17.657
Kaantymisreitti	1.653	1.980	3.722

Table 7: Gas Concetrations Measured during the campaign and averaged geometrically

Location	CO_2	CO_2 STD	NO_X	NO_X STD
North Tunnel	477.67	1.157	0.7908	2.405
Paasikiventie	408.51	1.056	0.1761	1.957
Risteys	414.83	1.074	0.2974	2.101
Moottoritie	408.59	1.036	0.1551	2.023
Kaantymisreitti	394.46	1.029	0.0952	1.989
Moottoritie 2	396.89	1.029	0.1379	2.057
Risteys 2	410.26	1.078	0.2348	2.302
Paasikiventie 2	402.13	1.040	0.1618	1.748
South Tunnel	453.81	1.122	0.5799	2.214
Kaantymisreitti	402.01	1.073	0.1753	2.554
Background	385.49	1.010	0.0357	1.133

APPENDIX B: FIGURES

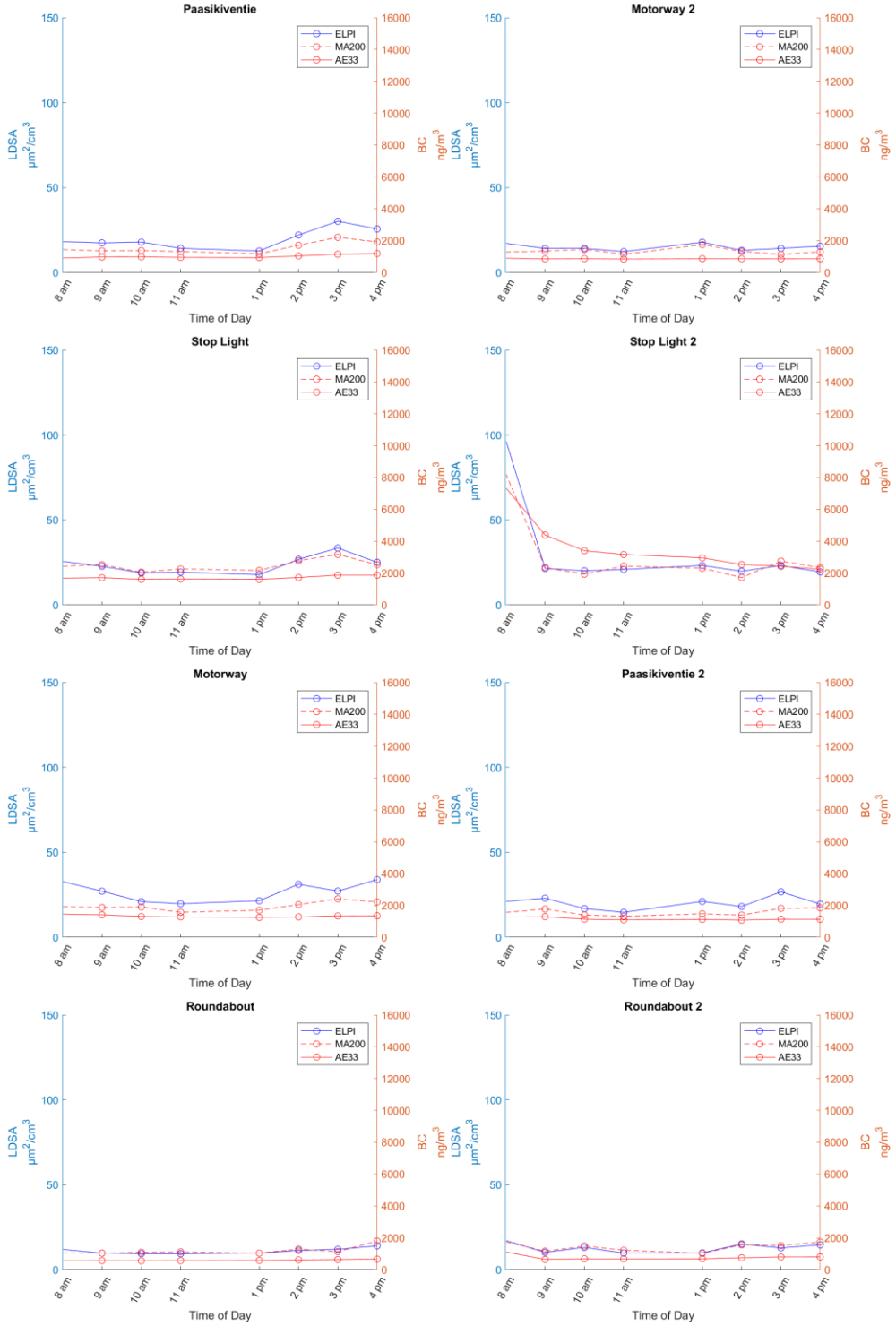

Figure 15: LDSA and Black Carbon all locations besides North and South tunnel. Evolution of concentration is shown throughout the day. Averaged geometrically